Talanta 308 (2026) 129836

Contents lists available at ScienceDirect

Talanta

journal homepage: www.elsevier.com/locate/talanta

A polyA-mediated AuNPs/MmC self-supporting electrochemical biosensor for amplification-free detection of crown-of-thorns starfish environmental DNA

Junjie Zeng [a,1], Chaoxin Zhang [a,1], Shaopeng Wang [a], Man Zhang [a], Zhenghua Chen [a,*], Kefu Yu [a], Liwei Wang [a,b,**], Honglei Jiang [a]

[a] School of Resources, Environment and Materials, Guangxi Laboratory on the Study of Coral Reefs in the South China Sea, School of Marine Sciences, School of Chemistry and Chemical Engineering, Guangxi University, Nanning, 530004, China
[b] Nansha Islands Coral Reef Ecosystem National Observation and Research Station, Guangzhou, 510300, China

ARTICLE INFO

Keywords:
Crown-of-thorns starfish
Environmental DNA
PolyA self-assembled monolayer
Electrochemical biosensor
Self-supporting
Early warning

ABSTRACT

The crown-of-thorns starfish (COTS) is a major predator on coral reefs, and its outbreaks can cause severe degradation of coral ecosystems, highlighting the critical importance of its early detection. Existing monitoring techniques offer limited spatial coverage, and available environmental DNA (eDNA)-based electrochemical biosensors are constrained by either low sensitivity or require complex nucleic acid amplification. To overcome these constraints, we construct a novel electrochemical biosensor that integrates a polyadenine (polyA) self-assembled monolayer with a self-supporting AuNPs-doped multiscale mesoporous carbon (AuNPs/MmC) electrode. The synergistic combination of a three-dimensional porous substrate for enhanced electron transport, polyA-mediated high-density probe immobilization, and enzymatic signal amplification enables early and precise detection of COTS without nucleic acid amplification. The sensor demonstrates a wide detection range from 0.1 pM to 1000 pM, a low detection limit of 8.82 fM, and good correlation ($R^2 = 0.972$). It shows excellent selectivity, reproducibility (cv $< 5\%$), and regenerability. The sensor demonstrated accuracy consistent with PCR methods in both aquarium experiments and actual sample testing ($P > 0.05$), along with better field applicability and cost-effectiveness. This technique is sensitive, specific, economical, and simple to use, offering significant value for early COTS detection and coral reef conservation.

1. Introduction

The crown-of-thorns starfish (COTS) is a keystone predator in Indo-Pacific coral reef ecosystems, and its population outbreaks can cause a drastic reduction in coral cover [1,2]. For instance, the Great Barrier Reef region saw an approximate 50.7% decline in its average hard coral cover between 1985 and 2012, largely due to recurrent COTS outbreaks [3,4]. However, Long-term monitoring of the Great Barrier Reef has confirmed that COTS outbreaks remain a primary driver of coral reef degradation throughout the 2010s and 2020s, with unmanaged outbreaks driving sector-wide coral cover losses of up to 50% during the system's 4th outbreak wave (2011–present) [5]. Unlike climate-driven coral bleaching, in which surviving corals can recover under favorable conditions, COTS predation inflicts irreversible whole-colony coral mortality and severely erodes reefs' natural recovery capacity even in the wake of other disturbance events, representing a persistent threat to coral reef ecosystem resilience [6–8]. Currently, the international community primarily relies on remotely operated vehicles (ROVs) and manned diving surveys for COTS tracking and quantitative assessment [9,10]. However, these methods are costly and ineffective at detecting COTS juveniles, provide limited spatial coverage, and fail to accurately track COTS distribution and dynamics in the water column. Consequently, effective monitoring and early warning remain significant challenges in coral reef conservation. In recent years, environmental

* Corresponding author.
** Corresponding author. School of Resources, Environment and Materials, Guangxi Laboratory on the Study of Coral Reefs in the South China Sea, School of Marine Sciences, School of Chemistry and Chemical Engineering, Guangxi University, Nanning, 530004, China.
E-mail addresses: chen.zhenghua@163.com (Z. Chen), wangliwei0427@163.com (L. Wang).
[1] These authors contributed equally to this work.

https://doi.org/10.1016/j.talanta.2026.129836
Received 8 January 2026; Received in revised form 22 March 2026; Accepted 13 April 2026
Available online 15 April 2026

DNA (eDNA)-based detection technology has emerged as a promising new approach for marine biomonitoring [11,12]. Uthicke et al. [13] employed droplet digital PCR (ddPCR) to detect COTS eDNA, demonstrating its potential for monitoring population dynamics and providing early warning of outbreaks, thereby supplementing or replacing traditional survey methods. Nevertheless, despite its high sensitivity, PCR technology is constrained by its dependence on laboratory settings, cumbersome procedures, and relatively high cost, making it difficult to meet the demands for rapid, large-scale, and high-frequency field monitoring [14]. Thus, there is a pressing need to develop a new eDNA detection method that is suitable for field application.

Electrochemical biosensors are promising for eDNA detection owing to their exceptional responsiveness, fast analysis, cost-effectiveness, compact design, and ease of operation [15,16]. Wang et al. [17] reported the first electrochemical biosensor capable of detecting COTS eDNA with a limit of detection (LOD) of 0.147 ng μL^{-1}, providing a basis for early on-site warning. Subsequently, Zhang et al. [18] introduced a cascade amplification strategy based on catalytic hairpin assembly (CHA) and hybridization chain reaction (HCR), which further decreased the LOD to 18.4 fM. Furthermore, Wen et al. [19] significantly enhanced the sensor accuracy and reliability by integrating Exonuclease III (Exo III)-assisted target recycling amplification with a dual-signal referencing strategy. Despite these advances, the aforementioned methods remain constrained by the operational complexity and contamination risks associated with nucleic acid amplification, as well as by the inherent drawbacks of conventional probe immobilization strategies. Most reported electrochemical DNA sensors rely on thiol-modified single-probe immobilization via Au–S bonds, which often suffer from uncontrollable probe orientation, severe steric hindrance, and poor stability in complex aqueous matrices. These issues lead to low target capture efficiency, gradual probe desorption, severe non-specific adsorption, and ultimately significant signal fluctuation, high background interference, and poor reproducibility in practical applications [20,21]. Consequently, developing an optimized probe immobilization strategy to address these interfacial limitations, while constructing an electrochemical biosensor capable of stable, reliable signal output without nucleic acid amplification, is of significant importance for achieving rapid, on-site detection of COTS eDNA.

In recent years, enhancing signal transduction and probe immobilization efficiency through material and electrode-interface design has been recognized as an effective approach to achieve high-sensitivity, amplification-free detection [22]. Among various strategies, self-supported three-dimensional porous materials offer excellent electron-transfer capabilities [23,24], while polyadenine (polyA) self-assembled monolayers, known for their high affinity to gold nanoparticles, enable high-density, oriented probe immobilization [25–27]. The integration of these two components offers a novel strategy for developing high-performance, amplification-free biosensors. In this study, we report the integration of a self-supported AuNPs/MmC porous electrode, a polyA-mediated high-density probe immobilization strategy, and enzyme-catalyzed signal amplification into a single amplification-free electrochemical biosensing platform. Unlike previous studies that employed these components in isolation, our approach leverages their synergistic interplay—the porous carbon enhances electron transfer and provides abundant surface area, polyA ensures oriented and dense probe packing, and HRP catalysis amplifies the detection signal—enabling femtomolar-level detection of COTS eDNA without nucleic acid amplification. This integrated design not only improves sensitivity and stability but also provides a practically applicable strategy for field-deployable eDNA monitoring.

2. Experimental section

2.1. Reagents and instruments

All reagents and instruments employed are detailed in Supporting Information S-1. The corresponding DNA sequences are compiled in Table S1.

2.2. Synthesis of AuNPs/MmC

First, tetraethyl orthosilicate (TEOS, 1 mL) was added to a mixture of ethanol (50 mL), deionized water (1 mL), and ammonia solution (5 mL). The mixture was stirred continuously for 6 h at room temperature. The resulting SiO_2 particles were collected by centrifugation, washed three times with ethanol and deionized water, and dried under vacuum at 60 °C. The obtained SiO_2 (500 mg) was thoroughly ground and dispersed in ethylene glycol (25 mL). After sonication for 30 min, the dispersion was stirred for 12 h at room temperature to form a homogeneous suspension. This suspension was then transferred into a 6 cm glass culture dish and dried at 60 °C, yielding the SiO_2 opal template.

Subsequently, the SiO_2 opal template was placed at the bottom of a cylindrical mold lined with aluminum foil. A mixture of oxalic acid (25 mg) and furfural (1 mL) was injected into the mold, allowing it to infiltrate the interstitial voids of the template. After aging at 90 °C for 72 h, a dark monolithic composite was obtained (Fig. S1). The composite underwent carbonization in an argon atmosphere (heating rate: 10 °C min^{-1}), with a 3 h hold at 200 °C followed by a 3 h dwell at 900 °C. The resultant composite was then etched in 6 M NaOH for 72 h to remove the SiO_2 template. After thorough washing with deionized water and drying, the MmC was obtained.

Finally, the as-prepared MmC was immersed in 40 mL of deionized water. Under stirring, $HAuCl_4$ solution (1 mL, 0.01 M) and glutathione (1 mL) were added dropwise, followed by stirring for 10 min. Then, after adding $NaBH_4$ solution (1 mL, 0.1 M), the reaction was allowed to proceed with stirring for 30 min at room temperature. Following a thorough wash with deionized water, the product was dried under vacuum at 60 °C to obtain the AuNPs/MmC.

2.3. Construction of the biosensor

In this study, AuNPs/MmC was directly employed as a self-supporting electrode (AuNPs/MmC SSE). First, the electrode was introduced into a 0.1 μM polyA-CP solution for overnight incubation at 4 °C. It was then thoroughly rinsed with deionized water to remove any unbound probes. Subsequently, to block nonspecific binding sites, the electrode was incubated with a 0.1 mM MCH solution for 30 min, followed by another deionized water wash to remove residual MCH. Finally, the modified AuNPs/MmC SSE was stored at 4 °C for subsequent electrochemical measurements.

2.4. Electrochemical measurement

First, a 0.1 μM biotin-modified reporter probe (RP) was mixed with varying concentrations of the target DNA in a hybridization buffer. The mixture was heated to 80 °C for 5 min, then equilibrated to ambient temperature for 20 min to facilitate complete hybridization and complex formation. Subsequently, the polyA-CP-modified SSE was immersed in the hybridization solution described above and incubated at 37 °C for 100 min to facilitate the specific binding of the target DNA to the capture probes anchored on the sensor surface. After removal, the electrode was washed with washing buffer. It was then incubated in a solution containing 0.5 U mL^{-1} of avidin-labeled horseradish peroxidase (avidin-HRP) at room temperature for 20 min. Finally, following another wash with washing buffer, the electrode could proceed to electrochemical detection.

A portable electrochemical workstation was employed to perform all measurements in a 3,3′,5,5′-Tetramethylbenzidine (TMB) substrate solution containing H_2O_2. Cyclic voltammetry (CV) was conducted with the following parameters: a potential scan ranges from 0 to 0.8 V, a scan rate of 0.05 V s^{-1}, and a sampling interval of 1 mV. Electrochemical impedance spectroscopy (EIS) was conducted over frequencies from 10^4

Hz to 0.1 Hz. For chronoamperometry (I-t) measurements, a constant potential of −200 mV was applied with a scan rate of 30 mV s^{-1}. The steady-state current recorded at 120 s was used as the output signal.

Buffer solutions used in this work are as follow: immobilization buffe (10 mM Tris-HCl, 1 mM EDTA, 1 mM NaCl, pH 7.0), washing buffer (10 mM Na_2HPO_4, 10 mM KH_2PO_4, 2.7 mM KCl, 137 mM NaCl, pH 7.4) and hybridization buffer (10 mM PBS, 20 mM $MgCl_2$, pH 7.4). Besides, 5 mM $[Fe(CN)_6]^{3-/4-}$ solution containing 0.1 M KCl was used for CV and EIS test. All the above buffer solutions were prepared with ultrapure water from a Millipore water purification system (18.2 MΩ, Milli-Q, Millipore).

2.5. Actual sample processing procedure

In April 2024, we conducted a field ecological survey of coral reefs in the Xisha Islands in the South China Sea. Guided by historical outbreak records, seawater samples were collected from eight selected sites (S1 ~ S8). Site-specific information is compiled in Table S2. At each site, a pre-cleaned organic glass water sampler, pre-treated with 10% sodium hypochlorite solution and thoroughly rinsed, was used to collect 5 L of seawater. The collected seawater was then filtered through a 0.2 μm polycarbonate (PC) membrane. After filtration, the membrane was transferred to −80 °C storage. eDNA was extracted following the procedure described in Supporting Information S-1. The enriched eDNA samples were analyzed using the developed biosensor, with each sample measured in triplicate.

3. Results and discussion

3.1. Detection mechanism of the biosensor

Scheme 1a illustrates the synthesis process of AuNPs/MmC nanocomposites via a template-assisted method and in situ reduction. Scheme 1b summarizes the assembly and detection mechanism of the sensor. Importantly, the enhancement strategy relies on signal amplification at the transducer interface rather than on nucleic acid amplification of the target. The signal enhancement arises from a multi-level synergistic strategy integrating three complementary amplification sources: (1) porous electrode-based signal enhancement—the SSE features a three-dimensional interconnected carbon network, providing a large effective surface area for probe immobilization while facilitating rapid electron transfer [28]; (2) polyA-mediated interfacial signal enhancement—the length of the polyA sequence enables precise and direct modulation of surface coverage; longer polyA blocks inherently reduce probe density due to their greater spatial occupancy, thereby avoiding the issues of excessive probe crowding commonly associated with thiolated DNA and the difficulty in precisely controlling the stoichiometry of mixed SAMs. Moreover, the polyA segment preferentially anchors to the AuNP surface and orients the recognition sequence upright, increasing the lateral spacing between adjacent probes while minimizing steric hindrance [29–31]. This synergistic combination of density modulation and oriented immobilization significantly enhances hybridization efficiency and kinetics; (3) enzymatic signal enhancement—following target binding, the biotin-labeled RP is captured,

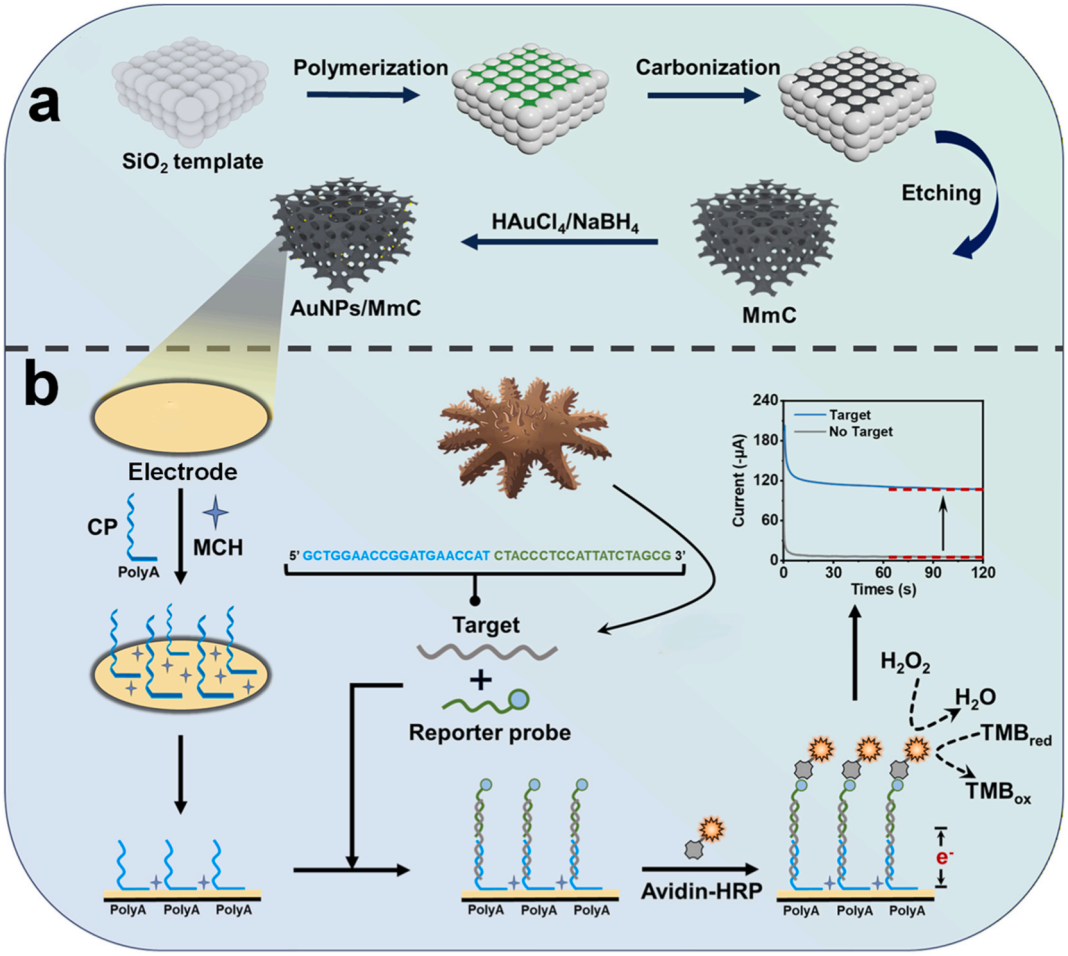

Scheme 1. (a) Schematic diagram of the preparation process for AuNPs/MmC, (b) Schematic illustration of the polyA-enhanced self-supporting electrochemical biosensor for detecting COTS.

forming a stable "sandwich" complex. This complex subsequently recruits avidin-HRP via biotin-avidin interaction. In the presence of H_2O_2, each HRP molecule catalyzes the oxidation of multiple TMB substrates, generating a greatly amplified electrochemical current. By synergistically integrating these three signal enhancement mechanisms, the sensor enables precise detection of COTS eDNA without the need for nucleic acid amplification.

3.2. Characterization of AuNPs/MmC

The morphology and structure of AuNPs/MmC were first characterized by scanning electron microscope (SEM). As shown in Fig. 1a, AuNPs/MmC exhibits a three-dimensional interconnected carbon network with a dense porous architecture, a structural feature that is critical for achieving high sensitivity and rapid response in electrochemical biosensing. Transmission electron microscopy (TEM) further revealed that AuNPs are uniformly dispersed on the graphitized carbon layers without significant aggregation (Fig. 1b). This uniformity ensures consistent polyA anchoring sites across the electrode surface, contributing to reproducible probe immobilization and stable sensor performance [32,33]. High-resolution TEM (HR-TEM) images show clear lattice fringes with an interplanar spacing of 0.23 nm (Fig. 1c), corresponding to the Au (111) plane. Meanwhile, energy-dispersive X-ray spectroscopy (EDS) mapping confirmed the homogeneous distribution of C, O, and Au elements within the material (Fig. 1d), which is consistent with the survey spectrum (Fig. S2).

As shown in Fig. 1e, X-ray diffraction (XRD) analysis revealed characteristic diffraction peaks corresponding to the (002) and (101) planes of graphitic carbon [34,35], along with distinct peaks at 2θ = 38.2°, 44.4°, 64.6°, and 77.5°, assigned to the (111), (200), (220), and (311) crystal planes of Au [36,37], respectively. These results confirm the successful loading of AuNPs without compromising the carbon framework. The high-resolution C 1s spectrum (Fig. 1f) shows peaks corresponding to C–C/C═C, C–O, and carboxyl functional groups, while the O 1s spectrum (Fig. 1g) reveals peaks attributable to C═O, C–O, and O–H bonds. The presence of oxygen-containing functional groups enhances interfacial wettability, ensuring higher electrochemical accessibility of surface-active sites in aqueous electrolytes, thereby improving the response sensitivity of the sensor [38]. The Au 4f spectrum (Fig. 1h) exhibits two peaks at 83.8 eV and 87.7 eV, corresponding to the $4f_{7/2}$ and $4f_{5/2}$ states of metallic Au^0, with a spin-orbit splitting of 3.7 eV [39], further confirming the successful deposition of AuNPs.

The specific surface area and pore structure of AuNPs/MmC were characterized by N_2 adsorption-desorption isotherms. As shown in Fig. 1i, the material exhibits a typical type-IV isotherm with an H_2-type hysteresis loop, characteristic of mesoporous materials [40,41]. The Brunauer-Emmett-Teller (BET) specific surface area was calculated to be 227 $m^2\ g^{-1}$. This high surface area provides abundant active sites for polyA probe immobilization, thereby increasing capture probe density and enhancing target recognition efficiency and signal output. The pore-size distribution curve (Fig. S3) shows two main peaks at 2.78 nm and 6.41 nm, indicating a hierarchical mesoporous structure that facilitates rapid diffusion of target molecules and electrolyte ions, thereby further promoting hybridization kinetics and electron transfer.

In summary, the combination of high specific surface area, hierarchical mesoporous structure, and favorable surface chemistry endows AuNPs/MmC with superior probe-loading capacity, efficient electron transfer, and stable interfacial properties. These structural advantages

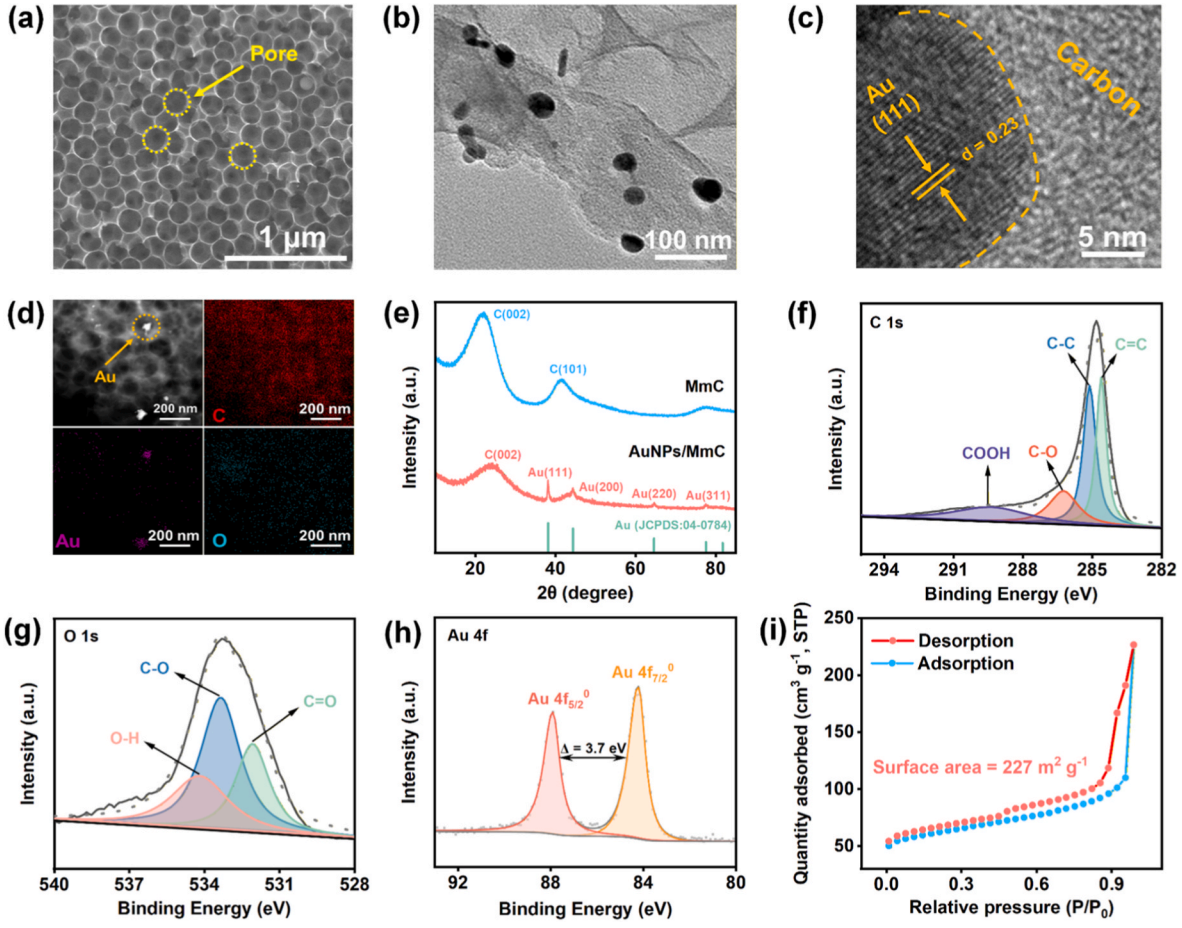

Fig. 1. (a) SEM image, (b) TEM image, and (c) HR-TEM image of AuNPs/MmC. (d) EDS elemental mapping spectrum of AuNPs/MmC. (e) XRD spectrum of AuNPs/MmC. (f) High-resolution spectra of C 1s, (g) O 1s, and (h) Au 4f. (i) N_2 adsorption-desorption isotherm of AuNPs/MmC.

establish a robust material foundation for constructing high-performance electrochemical biosensors with high sensitivity, good reproducibility, and reliable field applicability.

3.3. Feasibility analysis of the sensor

As shown in Fig. 2a, the AuNPs/MmC self-supporting electrode (SSE) exhibits a coin-like structure with uniform thickness and a smooth surface, approximately 2 cm in diameter. Fig. 2b illustrates the portable electrochemical device for COTS detection, which is based on a three-electrode system comprising an SSE working electrode, an Ag/AgCl reference electrode, and a Pt sheet counter electrode.

The stepwise assembly process of the sensor was characterized using EIS. As depicted in Fig. 2c, MmC exhibited an exceptionally low charge transfer resistance (Rct), which attributed to its three-dimensional framework and porous structure, which effectively facilitated electron transfer. Following the incorporation of AuNPs, the Rct of AuNPs/MmC further decreased, since the AuNPs can provide additional electrochemical active sites, thereby accelerating the interfacial charge transfer process [42]. Subsequently, the polyA-CP was grafted onto the electrode via the high-affinity interaction between polyA and Au. The negatively charged phosphate backbone induced electrostatic repulsion towards $[Fe(CN)_6]^{3-/4-}$ ions, leading to a significant increase in Rct. Further introduction of MCH to block non-specific sites, the Rct continued to increase. Lastly, after the attachment of both the target DNA and the reporter probe to the electrode surface, the Rct reached its maximum value, which is primarily due to the introduction of a substantial negative charge. These EIS changes validated the successful stepwise assembly of the sensor. CV and I-t further investigated the electrochemical behavior of the sensor in TMB-H_2O_2 substrates. Without target DNA, CV curve exhibited two pairs of characteristic redox peaks at the electrode. However, with target DNA, the "sandwich" double-stranded structure anchored HRP to the electrode surface via biotin-conjugated avidin. Under HRP catalysis, the reduction peak current of TMB was markedly enhanced (Fig. 2d). Correspondingly, the I-t curve (Fig. 2e) showed a significantly amplified steady-state current signal when the target DNA is present, resulting from the efficient catalytic reaction of TMB-H_2O_2 by HRP, consistent with the increased reduction current observed in the CV. These results demonstrated that the electrochemical biosensor based on AuNPs/MmC SSE modified with polyA self-assembled monolayers can effectively achieve specific recognition and signal transduction of target DNA, exhibiting feasibility and promising potential for COTS detection.

3.4. Evaluation of sensor performance

The analytical performance of the constructed sensor was evaluated by chronoamperometry under optimized experimental conditions. As shown in Fig. 3a, the sensor response current gradually increased as the target DNA concentration varied from 0.1 pM to 1000 pM. The current at 120 s was used as the quantitative signal to establish a calibration curve for different concentrations of target DNA (Fig. 3b). The results show that the relationship between the current signal and the target DNA concentrations follows a power-law function, as expressed in Equation (1):

$$y = 21.571x^{0.224} \left(R^2 = 0.972\right) \quad (1)$$

Based on the standard formulas for detection and quantification limits [43,44], the sensor achieved a limit of detection (LOD) of 8.82 fM (0.11 fg μL^{-1}) and a limit of quantification (LOQ) of 69.63 fM. Compared with previously reported methods (Table S3), this sensor demonstrates higher detection sensitivity. In contrast to biosensors employing a single-probe strategy, our approach integrated a three-dimensional porous substrate for enhanced electron transfer, polyA-mediated high-density probe immobilization, and enzymatic signal amplification, collectively achieving an LOD at the femtomolar level. Furthermore, compared with other reported nucleic acid amplification-free biosensors, this sensor offers improved detection sensitivity and stability through refined interface design and signal transduction mechanisms, while maintaining operational simplicity.

Selectivity is a key metric for evaluating biosensor performance [45].

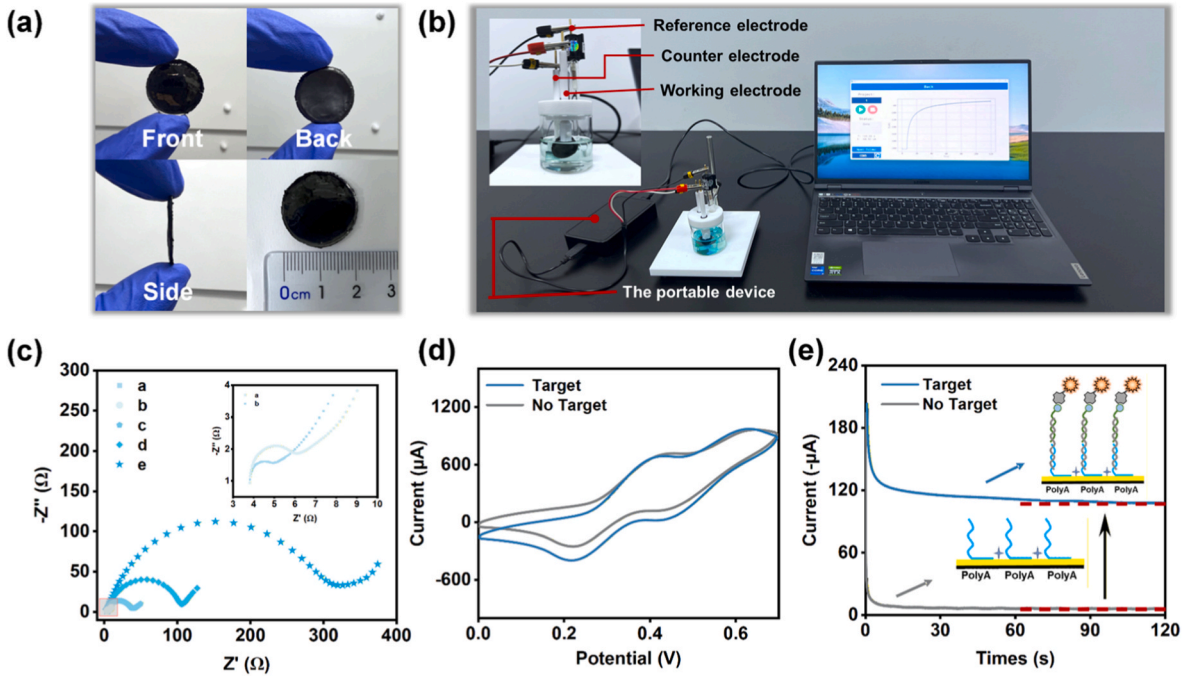

Fig. 2. (a) Presents digital images of the front, back, and side views of the AuNPs/MmC self-supporting electrode, with its diameter annotated. (b) The portable device employed for electrochemical analysis. (c) EIS curves of different modified electrodes: a, MmC; b, AuNPs/MmC; c, polyA10-CP/AuNPs/MmC; d, MCH/polyA10-CP/AuNPs/MmC; e, reporter probe/target/MCH/polyA10-CP/AuNPs/MmC. (d) CV curve and (e) I-t curve of TMB analyzed using polyA10-CP: with target (1 nM), without target (hybridization buffer).

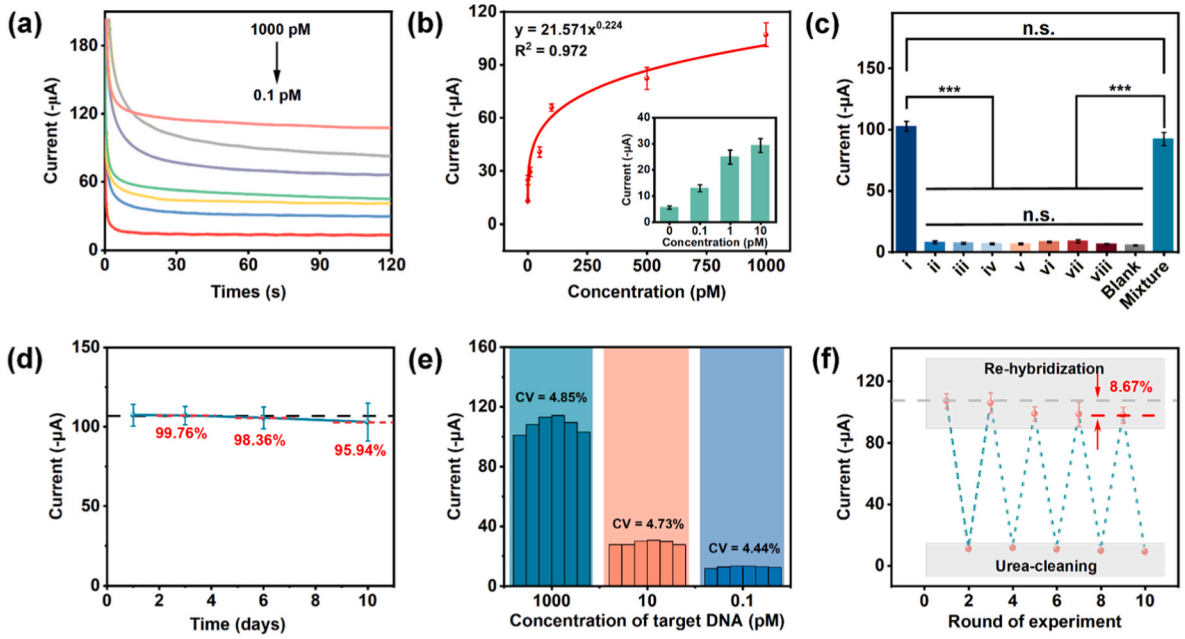

Fig. 3. (a) I-t curves measured using the electrochemical biosensor, and (b) corresponding calibration curves for different target DNA concentrations (0.1 pM, 1 pM, 10 pM, 50 pM, 100 pM, 500 pM, and 1000 pM). (c) Selectivity assessment of the biosensor (i: COTS, ii: *Linckia laevigata*, iii: *Culcita novaeguineae*, iv: *Montastrea curta*, v: *Pocillopora damicornis*, vi: *Platygyra sinensis*, vii: *Naso lituratus*, viii: *Lethrinus erythropterus*). (d) Stability assessment of the biosensor. (e) Repeatability assessment of the biosensor (corresponding to target concentrations of 1000 pM, 10 pM, and 0.1 pM respectively). (f) Regeneration assessment of the biosensor. Error bars denote the standard deviation of three parallel experiments ($n = 3$). ***$P < 0.001$, *n. s.* > 0.05.

To verify the specificity of the constructed sensor, selectivity tests were performed using genomic DNA from seven common species associated with South China Sea coral reef areas as potential interferents (*Linckia laevigata*, *Culcita novaeguineae*, *Montastrea curta*, *Pocillopora damicornis*, *Platygyra sinensis*, *Naso lituratus*, and *Lethrinus erythropterus*) (Fig. S5). As shown in Fig. 3c, when only an interferent was present, there was no significant difference between the current signal detected by the sensor and that of the blank control ($P > 0.05$). In contrast, both the target DNA alone and its mixture with interferents induced a significantly amplified signal, showing a statistically significant difference compared to the interference groups ($P < 0.001$). This result is primarily attributed to the high sequence-specific recognition capability of the polyA-CP towards the target DNA.

To evaluate the storage stability of the constructed sensor, it was stored at 4 °C and tested periodically. As shown in Fig. 3d, the current signal remained stable with no significant decay after 3 days of storage. The signal retention rate was 98.36% after 6 days, and only a 4.06% decrease was observed after 10 days, indicating excellent storage stability. The reproducibility of sensor fabrication and measurement was further investigated. Eighteen AuNPs/MmC SSEs were prepared in parallel and used to detect target DNA at three different concentrations: 1000 pM, 10 pM, and 0.1 pM. As shown in Fig. 3e, the coefficients of variation (cv) for these concentrations were 4.85%, 4.73%, and 4.44%, respectively, demonstrating good reproducibility. These results confirm that the sensor exhibits outstanding stability and reproducibility for COTS detection. Theses excellent performances are primarily attributed to the stable immobilization of polyA-CP on the electrode surface, the effective interfacial control by the self-assembled monolayer, and the inherent structural stability of the AuNPs/MmC SSE, which together ensure reliable sensor performance in practical applications.

The strong and stable self-assembly of polyA on the electrode surface allows the sensor to maintain the structural integrity of its interface even after repeated hybridization and denaturation cycles, thereby enabling sensor regeneration [46]. As shown in Fig. 3f and Fig. S6, the fabricated sensor was first tested for an initial measurement (Round 1). The sensor was then treated with urea solution concentration to denature the surface-bound "sandwich" complex, showing a background current signal (Round 2), indicating the effective removal of the captured DNA complex. The same electrode was subsequently used again to detect the same concentration of target DNA, and the current signal recovered to the initial level (Round 3), confirming the good regeneration capability of the sensor. After five consecutive regeneration cycles, the current signal decreased by only approximately 8.67% (Round 9), further demonstrating the reliable reusability of the sensor. These results prove that the polyA-CP possesses a stable conformation and strong surface binding affinity, which endows the sensor with excellent regenerability and helps reduce the cost per test. The single detection time for this sensor was calculated to be approximately 147 min, with a per-test cost of only $1.20. Compared with other detection methods (Table S4), this sensor shows clear advantages in both detection time and economic cost.

3.5. Accuracy verification

To validate the accuracy of the sensor in practical applications, an aquarium experiment was designed (Fig. 4a). First, quality control protocols were performed to monitor potential contamination during the eDNA enrichment operation. As shown in Fig. 4b, the current signal of the blank group was comparable to the background signal and significantly lower than that of the experimental group ($P < 0.001$), indicating no contamination occurred throughout the experiment and effectively avoiding false-positive interference. Subsequently, eDNA detection was conducted on water samples from aquariums without COTS (negative control, B1 ~ B3) and with COTS (B4 ~ B6). As shown in Fig. 4c, samples B4 ~ B6 generated a significantly enhanced current signal versus the negative control ($P < 0.001$) but did not differ significantly from the positive control ($P > 0.05$). In contrast, the signal of B1 ~ B3 remained consistent with the negative control ($P > 0.05$), confirming the reliability of the sensor for detecting COTS eDNA. To further confirm the accuracy of the sensor, a comparative analysis was performed using ddPCR as the gold-standard method. As shown in Fig. 4d, the results obtained with the sensor for both negative and positive samples showed no significant difference from the ddPCR results ($P >$

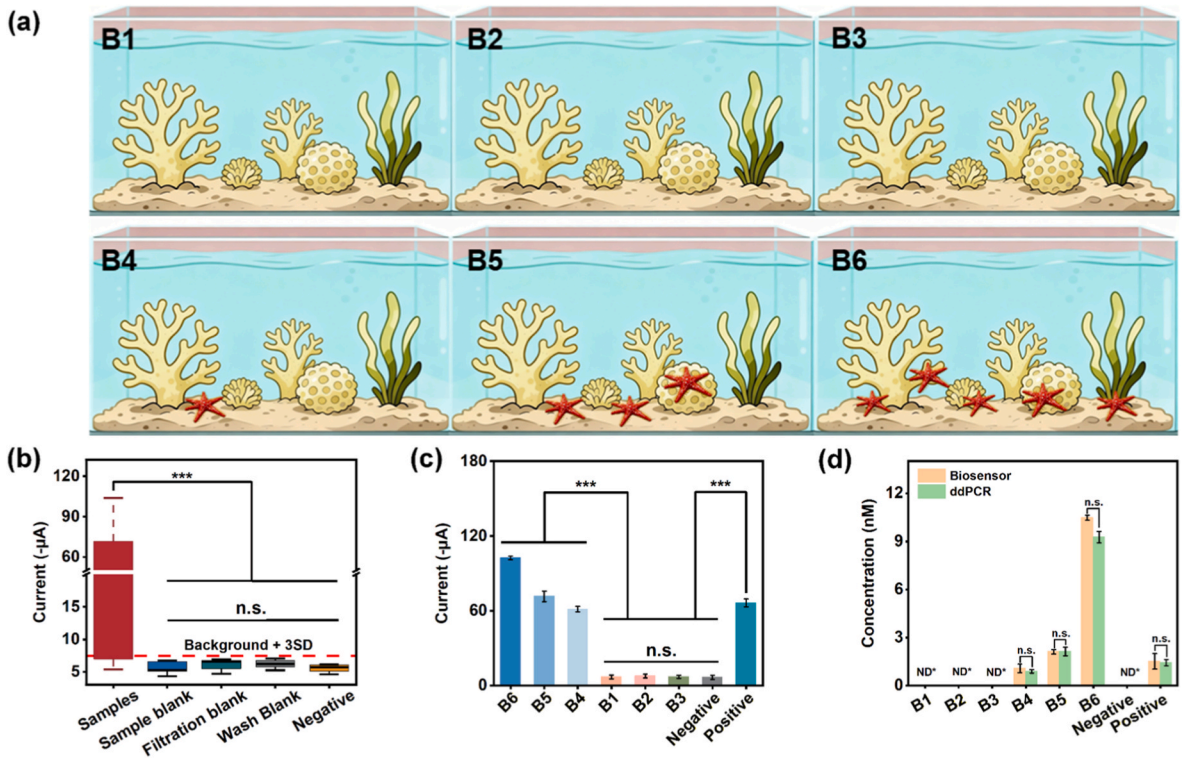

Fig. 4. (a) Schematic diagram of the aquarium experiment. B1 ~ B3: Negative control groups; B4 ~ B6: Positive control groups. (b) Box plot of biosensor test data from the blank control experiment. (c) Sensor detection results from the aquarium experiment. (d) Differential analysis of biosensor and ddPCR detection results. Error bars denote standard deviation from three parallel experiments ($n = 3$). ***$P < 0.001$, *n. s.* > 0.05, *ND** denotes not detected.

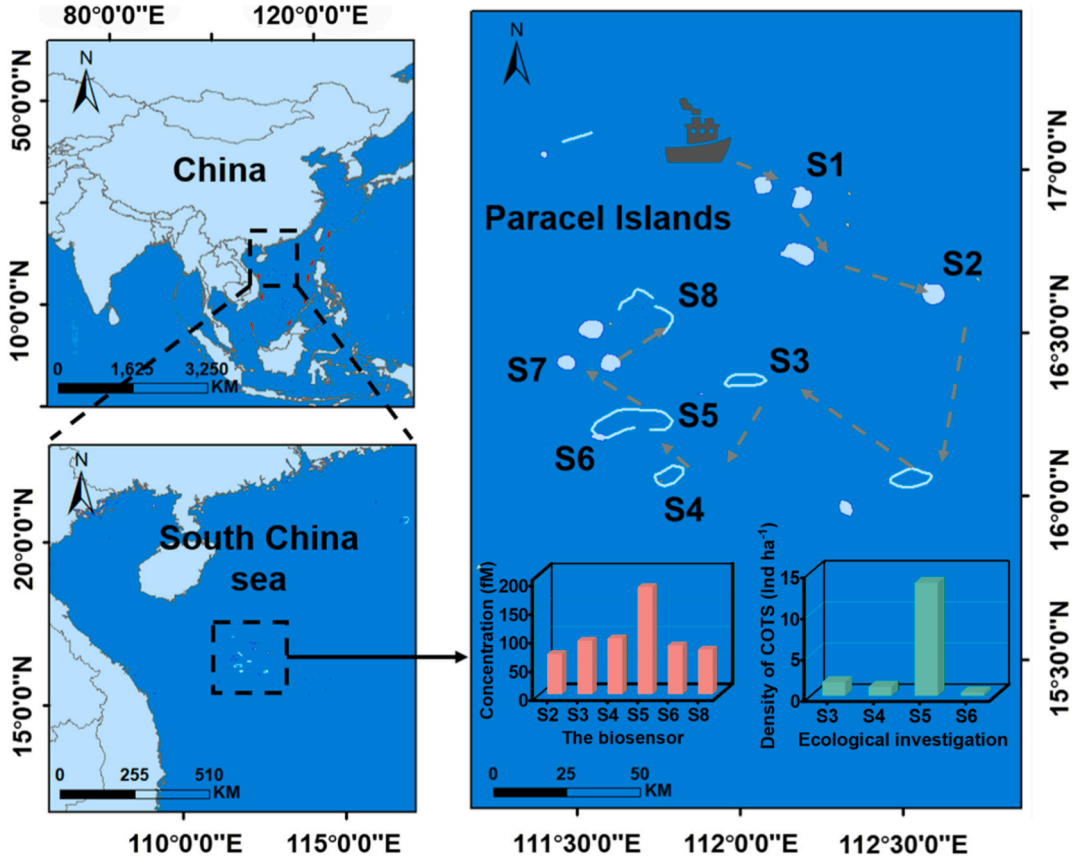

Fig. 5. Schematic map of the study area and sampling sites (S1 ~ S8). Bar charts represent COTS eDNA concentrations (biosensor measurements, left) and ecological survey densities (right) at each site. The map is drawn using a standard geographic coordinate system; see legend for scale.

0.05), demonstrating excellent agreement between the two methods. The sensor demonstrated reliable detection performance consistent with the standard method under simulated real-world conditions, indicating strong potential for field applications.

3.6. Actual sample detection

To evaluate the detection performance of the sensor in real-world complex environments, this study conducted COTS eDNA detection in the waters of the Xisha Islands in the South China Sea. Seawater collection, processing, and eDNA extraction for all samples followed strict quality control protocols (Supporting Information S-1, Fig. 4b) to ensure data reliability. As shown in Fig. 5, no adult COTS were recorded during the ecological survey at sites S1, S2, S7, and S8. However, the sensor still detected significant eDNA signals at sites S2 and S8 (Fig. 5, bar chart). This is primarily due to the detection limitations inherent in ecological surveys, which struggle to effectively identify smaller, cryptic, or coral-dwelling starfish larvae, potentially leading to omission [47]. In contrast, the sensor directly captures COTS eDNA from the water column, offering a more sensitive indication of presented COTS, irrespective of life stage or activity patterns. Notably, at sites where COTS were confirmed by ecological surveys (S3 ~ S6), the number of COTS per unit area and the eDNA concentration measured by the sensor showed similar trends (Fig. 5, bar chart). This suggests that eDNA concentration in water can, to some extent, reflect local population density of the target organism [48].

Comparative analysis was performed on the same batch of samples using qPCR. No significant difference was found between the eDNA concentrations obtained by the two methods ($P > 0.05$) (Table S5). Linear regression analysis indicated a high correlation between the two datasets (Pearson's r = 0.996; Fig. S7), confirming the excellent detection accuracy and reliability of the sensor even in complex real-world water samples. Compared with the PCR methods, the sensor maintains high accuracy while offering additional advantages such as lower cost, portability, and faster detection, providing a feasible technical support system for early monitoring and warning of COTS outbreaks.

4. Conclusion

In this study, a polyadenine-enhanced, porous carbon, self-supporting electrochemical biosensor was constructed for highly sensitive and specific detection of COTS eDNA. The core innovation is integrating three components into one sensing platform: a self-supported AuNPs/MmC porous electrode, a polyA-mediated high-density probe immobilization strategy, and enzyme-catalyzed signal amplification. Unlike previous amplification-free electrochemical DNA sensors that typically rely on only one or two of these features, our approach achieves a synergistic enhancement through their combination: the three-dimensional porous carbon framework facilitates efficient electron transfer, the polyA self-assembled monolayer enables oriented and high-density capture probe immobilization, and the HRP-catalyzed reaction provides robust signal amplification. This synergistic design enables femtomolar-level sensitivity (LOD = 8.82 fM) without the need for nucleic acid amplification, while maintaining a broad linear range (0.1 to 1000 pM, $R^2 = 0.972$). The sensor also exhibited excellent selectivity, reproducibility (cv < 5%), and stability, and could be regenerated for more than five cycles. Owing to its amplification-free nature, each assay requires only approximately 147 min and costs about $1.2, substantially reducing both time and expense compared to PCR-based methods. Both aquarium experiments and actual sample testing demonstrated that the sensor achieved high consistency with PCR methods ($P > 0.05$), confirming its good accuracy and reliability in real-world environments. Notably, the sensor successfully detected COTS eDNA at sites where visual surveys failed to identify cryptic or juvenile individuals, underscoring its value as an early warning tool capable of detecting COTS at very low pre-outbreak population densities, directly informing COTS control and coral reef conservation strategies—including long-term reef management via water quality improvement and marine protected area establishment, biological control through natural predator release, and targeted manual removal for direct intervention—and enabling proactive rather than reactive management as a practical, field-deployable platform for coral reef protection and COTS outbreak prevention. Future efforts could focus on developing fully integrated portable devices to enable rapid on-site decision-making for coral reef conservation.

CRediT authorship contribution statement

Junjie Zeng: Writing – original draft, Methodology, Investigation, Data curation, Conceptualization. **Chaoxin Zhang:** Writing – review & editing, Formal analysis, Data curation. **Shaopeng Wang:** Software, Resources. **Man Zhang:** Writing – review & editing. **Zhenghua Chen:** Writing – review & editing. **Kefu Yu:** Writing – review & editing. **Liwei Wang:** Writing – review & editing, Supervision, Resources, Funding acquisition. **Honglei Jiang:** Data curation.

Declaration of competing interest

The authors declare that they have no known competing financial interests or personal relationships that could have appeared to influence the work reported in this paper.

Acknowledgment

This work was supported by the National Natural Science Foundation of China of P. R. China (No. 22564003, 42501364), the Guangxi Major Talent Project (Bagui Young Elite Talents), the Self-Topic Project of Guangxi Laboratory on the Study of Coral Reefs in the South China Sea, Nanning 530004, China (No. GXLSCRSCS2023102), the Open Fund of Nansha Islands Coral Reef Ecosystem National Observation and Research Station (No. NSICR24204), and Guangxi First Batch of Young Talent Nurturing Universal Support Policy Research Startup Fund (Recipient: Honglei Jiang). We are grateful to Professor Xiangrong Xu for her guidance on the detection and analytical methods during the revision of this manuscript. We also gratefully acknowledge the valuable assistance provided by the Sansha Track Ocean Coral Reef Conservation Research Institute for their help in collecting specimens of COTS.

Appendix B. Supplementary data

Supplementary data to this article can be found online at https://doi.org/10.1016/j.talanta.2026.129836.

Data availability

Data will be made available on request.

References

[1] F.J. Kroon, D.R. Barneche, M.J. Emslie, Fish predators control outbreaks of crown-of-thorns starfish, Nat. Commun. 12 (2021) 6986, https://doi.org/10.1038/s41467-021-26786-8.

[2] M.R. Hall, K.M. Kocot, K.W. Baughman, S.L. Fernandez-Valverde, M.E.A. Gauthier, W.L. Hatleberg, A. Krishnan, C. McDougall, C.A. Motti, E. Shoguchi, T. Wang, X. Xiang, M. Zhao, U. Bose, C. Shinzato, K. Hisata, M. Fujie, M. Kanda, S. F. Cummins, N. Satoh, S.M. Degnan, B.M. Degnan, The crown-of-thorns starfish genome as a guide for biocontrol of this coral reef Pest, Nature 544 (2017) 231–234, https://doi.org/10.1038/nature22033.

[3] É.E. Plagányi, R.C. Babcock, J. Rogers, M. Bonin, E.B. Morello, Ecological analyses to inform management targets for the culling of crown-of-thorns starfish to prevent coral decline, Coral Reefs 39 (2020) 1483–1499, https://doi.org/10.1007/s00338-020-01981-z.

[4] D.A. Westcott, C.S. Fletcher, F.J. Kroon, R.C. Babcock, E.E. Plagányi, M. S. Pratchett, M.C. Bonin, Relative efficacy of three approaches to mitigate crown-of-thorns star fish outbreaks on Australia's great barrier reef, Sci. Rep. 10 (2026) 12594, https://doi.org/10.1038/s41598-020-69466-1.

[5] S.A. Matthews, D.H. Williamson, R. Beeden, M.J. Emslie, R.T.M. Abom, D. Beard, M. Bonin, P. Bray, A.R. Campili, D.M. Ceccarelli, L. Fernandes, C.S. Fletcher, D. Godoy, C.R. Hemingson, M.J. Jonker, B.J. Lang, S. Morris, E. Mosquera, G. L. Phillips, T.H. Sinclair-Taylor, S. Taylor, D. Tracey, J.C. Wilmes, R. Quincey, Protecting great barrier reef resilience through effective management of crown-of-thorns starfish outbreaks, PLoS One 19 (2024), https://doi.org/10.1371/journal.pone.0298073 e0298073-.

[6] Y.-M. Bozec, K. Hock, R.A.B. Mason, M.E. Baird, C. Castro-Sanguino, S.A. Condie, M. Puotinen, A. Thompson, P.J. Mumby, Cumulative impacts across Australia's great barrier reef: a mechanistic evaluation, Ecol. Monogr. 92 (2022) e01494, https://doi.org/10.1002/ecm.1494.

[7] M.J. Emslie, D.M. Ceccarelli, M. Logan, M.I. Blandford, P. Bray, A. Campili, M. J. Jonker, J.G. Parker, T. Prenzlau, T.H. Sinclair-Taylor, Changing dynamics of great barrier reef hard coral cover in the anthropocene, Coral Reefs 43 (2024) 747–762, https://doi.org/10.1007/s00338-024-02498-5.

[8] M.J. Emslie, M. Logan, P. Bray, D.M. Ceccarelli, A.J. Cheal, T.P. Hughes, K. A. Johns, M.J. Jonker, E. v Kennedy, J.T. Kerry, C. Mellin, I.R. Miller, K. Osborne, M. Puotinen, T. Sinclair-Taylor, H. Sweatman, Increasing disturbance frequency undermines coral reef recovery, Ecol. Monogr. 94 (2024) e1619, https://doi.org/10.1002/ecm.1619.

[9] M. Jyothimurugan, S. Pavithra, J. Deepika Roselind, Efficient underwater ecological monitoring with embedded AI: detecting crown-of-thorns starfish via DCGAN and YOLOv6, Front. Mar. Sci. 12–2025 (2025). https://www.frontiersin.org/journals/marine-science/articles/10.3389/fmars.2025.1658205.

[10] M.D.E. Haywood, D.P. Thomson, R.C. Babcock, R.D. Pillans, J.K. Keesing, M. Miller, W.A. Rochester, A. Donovan, R.D. Evans, G. Shedrawi, S.N. Field, Crown-of-thorns starfish impede the recovery potential of coral reefs following bleaching, Mar. Biol. 166 (2019) 99, https://doi.org/10.1007/s00227-019-3543-z.

[11] A. Koziol, M. Stat, T. Simpson, S. Jarman, J.D. DiBattista, E.S. Harvey, M. Marnane, J. McDonald, M. Bunce, Environmental DNA metabarcoding studies are critically affected by substrate selection, Mol. Ecol. Resour. 19 (2019) 366–376, https://doi.org/10.1111/1755-0998.12971.

[12] Y. Jiang, W. Zhao, Y. Zhu, S. Ma, M. Li, S. Zhang, K. Zou, An innovative approach for marine macro-organism monitoring: methodology and future perspectives of environmental DNA (eDNA) technology, Mar. Biol. 172 (2026), https://doi.org/10.1007/s00227-025-04609-4.

[13] S. Uthicke, M. Lamare, J.R. Doyle, eDNA detection of corallivorous seastar (Acanthaster cf. solaris) outbreaks on the great barrier reef using digital droplet PCR, Coral Reefs 37 (2018) 1229–1239, https://doi.org/10.1007/s00338-018-1734-6.

[14] Y. Hou, S. Chen, Y. Zheng, X. Zheng, J.-M. Lin, Droplet-based digital PCR (ddPCR) and its applications, TrAC, Trends Anal. Chem. 158 (2023) 116897, https://doi.org/10.1016/j.trac.2022.116897.

[15] Y. Zhang, H. Liu, S. Wang, H. Fu, Y. Xie, C. Zhang, M. Zhang, J. Lu, L. Wang, K. Yu, Advancements of the Vibrio coralliilyticus eDNA detection based on Co- Fe PBA-assisted biosensors for the rapid coral-disease warning, Biochem. Eng. J. 216 (2026) 109662, https://doi.org/10.1016/j.bej.2025.109662.

[16] B. Rafique, M. Iqbal, T. Mehmood, M.A. Shaheen, Electrochemical DNA biosensors: a review, Sens. Rev. 39 (2018) 34–50, https://doi.org/10.1108/SR-08-2017-0156.

[17] L. Wang, J. Xu, H. Liu, S. Wang, W. Ou, M. Zhang, F. Wei, S. Luo, B. Chen, S. Zhang, K. Yu, Ultrasensitive and on-site eDNA detection for the monitoring of crown-, Biosens. Bioelectron. 230 (2026) 115265, https://doi.org/10.1016/j.bios.2023.115265.

[18] Z. Wei, X. Zhang, Y. Chen, H. Liu, S. Wang, M. Zhang, H. Ma, K. Yu, L. Wang, A new strategy based on a cascade amplification strategy biosensor for, Sci. Total Environ. 927 (2026) 172258, https://doi.org/10.1016/j.scitotenv.2024.172258.

[19] B. Wen, Z. Zhu, J. Zeng, S. Wan, C. Zhang, Y. Chen, L. Wang, M. Zhang, K. Yu, A ratiometric electrochemical DNA biosensor for the detection of crown -of-thorns starfish eDNA, Bioelectrochemistry 168 (2026) 109162, https://doi.org/10.1016/j.bioelechem.2025.109162.

[20] Y. Wang, Z. Wang, Y. Shang, J. Wang, Z. Zhu, L. Xi, J. Xie, Q. Wu, Y. Shen, Y. Ding, Next-generation pathogen detection: exploring the power of nucleic acid amplification-free biosensors, Coord. Chem. Rev. 513 (2026) 215895, https://doi.org/10.1016/j.ccr.2024.215895.

[21] T. Cholko, C.-E.A. Chang, Modeling effects of surface properties and probe density for nanoscale biosensor design: a case study of DNA hybridization near surfaces, J. Phys. Chem. B 125 (2026) 1746–1754, https://doi.org/10.1021/acs.jpcb.0c09723.

[22] Y. Bai, P. Xu, S. Li, D. Wang, K. Zhang, D. Zheng, D. Yue, G. Zhang, S. He, Y. Li, H. Zou, Y. Deng, Signal amplification strategy of DNA self-assembled biosensor and typical applications in pathogenic microorganism detection, Talanta 272 (2026) 125759, https://doi.org/10.1016/j.talanta.2024.125759.

[23] X. Guan, P. Yang, S. Zhang, J. Guan, Z. Zhang, S. Yin, F. Han, Y. Xing, Study on the preparation of three-dimensional flexible self-supporting thick electrodes using phase transformation method and their electrochemical performance, J. Energy Storage 120 (2026) 116392, https://doi.org/10.1016/j.est.2025.116392.

[24] C. Zhou, P. Zhang, J. Liu, J. Zhou, W. Wang, K. Li, J. Wu, Y. Lei, L. Chen, Hierarchical $NiCo_2Se_4$ nanoneedles/nanosheets wit h N-doped 3D porous graphene architecture as free-standing anode for superior sodium ion batteries, J. Colloid Interface Sci. 587 (2026) 260–270, https://doi.org/10.1016/j.jcis.2020.12.015.

[25] D. Li, Z. Luo, H. An, E. Yang, M. Wu, Z. Huang, Y. Duan, Poly-adenine regulated DNA density on AuNPs to construct efficient DNA walker for microRNA-21 detection, Talanta 217 (2026) 121056, https://doi.org/10.1016/j.talanta.2020.121056.

[26] X. Hua, J. Fan, L. Yang, J. Wang, Y. Wen, L. Su, X. Zhang, Rapid detection of miRNA via development of consecutive adenines (poly, Biosens. Bioelectron. 198 (2026) 113830, https://doi.org/10.1016/j.bios.2021.113830.

[27] L. Wang, Y. Wen, X. Yang, L. Xu, W. Liang, Y. Zhu, L. Wang, Y. Li, Y. Li, M. Ding, S. Ren, Z. Yang, M. Lv, J. Zhang, K. Ma, G. Liu, Ultrasensitive electrochemical DNA biosensor based on a label-free assembling strategy using a triblock polyA DNA probe, Anal. Chem. 91 (2026) 16002–16009, https://doi.org/10.1021/acs.analchem.9b04757.

[28] M. Wang, H. Zhang, Y. Li, R. Liu, H. Yang, A three-dimensional co-continuous network structure polymer electrolyte with efficient ion transport channels enabling ultralong-life all solid-state lithium metal batteries, J. Energy Chem. 94 (2024) 635–645, https://doi.org/10.1016/j.jechem.2024.02.069.

[29] D. Zhu, P. Song, J. Shen, S. Su, J. Chao, A. Aldalbahi, Z. Zhou, S. Song, C. Fan, X. Zuo, Y. Tian, L. Wang, H. Pei, PolyA-Mediated DNA assembly on gold nanoparticles for thermodynamically favorable and rapid hybridization analysis, Anal. Chem. 88 (2016) 4949–4954, https://doi.org/10.1021/acs.analchem.6b00891.

[30] X. Hua, J. Fan, L. Yang, J. Wang, Y. Wen, L. Su, X. Zhang, Rapid detection of miRNA via development of consecutive adenines (polyA)-based electrochemical biosensors, Biosens. Bioelectron. 198 (2022) 113830, https://doi.org/10.1016/j.bios.2021.113830.

[31] L. Wang, H. Zhang, C. Wang, Y. Xu, J. Su, X. Wang, X. Liu, D. Feng, L. Wang, X. Zuo, J. Shi, Z. Ge, C. Fan, X. Mi, Poly-adenine-mediated spherical nucleic acids for strand displacement-based DNA/RNA detection, Biosens. Bioelectron. 127 (2019) 85–91, https://doi.org/10.1016/j.bios.2018.12.003.

[32] Y. Xue, Y. Wang, S. Feng, M. Yan, J. Huang, X. Yang, A dual-amplification mode and Cu-based metal-organic frameworks mediated electrochemical biosensor for sensitive detection of microRNA, Biosens. Bioelectron. 202 (2026) 113992, https://doi.org/10.1016/j.bios.2022.113992.

[33] W.-J. Shen, Y. Zhuo, Y.-Q. Chai, R. Yuan, Cu-Based metal–organic frameworks as a catalyst to construct a ratiome tric electrochemical aptasensor for sensitive lipopolysaccharide detec tion, Anal. Chem. 87 (2026) 11345–11352, https://doi.org/10.1021/acs.analchem.5b02694.

[34] S. Guan, J. Li, Y. Wang, Y. Yang, X. Zhu, D. Ye, R. Chen, Q. Liao, Multifunctional MOF-derived Au, Co-Doped porous carbon electrode for a wearable sweat energy harvesting-storage hybrid system, Adv. Mater. 35 (2026) e2304465, https://doi.org/10.1002/adma.202304465.

[35] M. Liu, L. Huang, Y. Duan, B. Gu, J. Li, H. Wei, W. Xue, Y. Jiang, C. Sun, Heating induced self-assemble pomegranate-like Fe3C@Graphite magnetic microspheres on amorphous carbon for high-performance microwave absorption, Compos. B Eng. 260 (2026) 110767, https://doi.org/10.1016/j.compositesb.2023.110767.

[36] R. Sakthivel, S.B. Prasanna, C.-L. Tseng, L.-Y. Lin, Y.-F. Duann, J.-H. He, R.-J. Chung, A sandwich-type electrochemical immunosensor for insulin detection Bas ed on Au-Adhered Cu_5 Zn_8 hollow porous carbon Nanocubes and AuNP deposited nitrogen-doped Holey graphene, Small 18 (2026) e2202516, https://doi.org/10.1002/smll.202202516.

[37] A.B. Ganganboina, N.K. Dega, H.L. Tran, W. Darmonto, R.-A. Doong, Application of sulfur-doped graphene quantum dots@gold-carbon nanosphere for electrical pulse-induced impedimetric detection of glioma cells, Biosens. Bioelectron. 181 (2026) 113151, https://doi.org/10.1016/j.bios.2021.113151.

[38] W. Yao, A. Hu, J. Ding, N. Wang, Z. Qin, X. Yang, K. Shen, L. Chen, Y. Li, Hierarchically ordered macro–mesoporous electrocatalyst with hydrophilic surface for efficient oxygen reduction reaction, Adv. Mater. 35 (2023) 2301894, https://doi.org/10.1002/adma.202301894.

[39] M. Caux, H. Menard, Y.M. AlSalik, J.T.S. Irvine, H. Idriss, Photo-catalytic hydrogen production over Au/g-C_3N<sub>4</su b>: effect of gold particle dispersion and morphology, Phys. Chem. Chem. Phys. 21 (2026) 15974–15987, https://doi.org/10.1039/c9cp02241d.

[40] Q. Lian, M.I. Konggidinata, Z.U. Ahmad, D.D. Gang, L. Yao, R. Subramaniam, E. Revellame, W.B. Holmes, M. Zappi, Combined effects of textural and surface properties of modified ordered mesoporous carbon (OMC) on BTEX adsorption, J. Hazard Mater. 377 (2026) 381–390, https://doi.org/10.1016/j.jhazmat.2019.05.079.

[41] M. Wei, F. Marrakchi, C. Yuan, X. Cheng, D. Jiang, F.F. Zafar, Y. Fu, S. Wang, Adsorption modeling, thermodynamics, and DFT simulation of tetracyclin e onto mesoporous and high-surface-area NaOH-activated macroalgae carb on, J. Hazard Mater. 425 (2026) 127887, https://doi.org/10.1016/j.jhazmat.2021.127887.

[42] M. Tavakkoli Yaraki, N.S. Rubio, A. Tukova, J. Liu, Y. Gu, L. Kou, Y. Wang, Spectroscopic identification of charge transfer of thiolated molecules on gold nanoparticles via gold nanoclusters, J. Am. Chem. Soc. 146 (2026) 5916–5926, https://doi.org/10.1021/jacs.3c11959.

[43] L. Liu, X. Zhou, Y. Lu, H. Shi, M. Ma, T. Yu, Triple functional small-molecule-protein conjugate mediated optical biosensor for quantification of estrogenic activities in water samples, Environ. Int. 132 (2026) 105091, https://doi.org/10.1016/j.envint.2019.105091.

[44] M. Idrees, M. Ayaz, R. Bibi, M.N. Khan, Fluorescence quenching of the probes L-Tryptophan and indole by anions in aqueous system, Anal. Sci. 36 (2026) 183–185, https://doi.org/10.2116/analsci.19p264.

[45] H. Moulahoum, F. Ghorbanizamani, The LOD paradox: when lower isn't always better in biosensor research and development, Biosens. Bioelectron. 264 (2026) 116670, https://doi.org/10.1016/j.bios.2024.116670.

[46] L. Li, L. Wang, Q. Xu, L. Xu, W. Liang, Y. Li, M. Ding, A. Aldalbahi, Z. Ge, L. Wang, J. Yan, N. Lu, J. Li, Y. Wen, G. Liu, Bacterial analysis using an electrochemical DNA

biosensor with Poly-Adenine-mediated DNA self-assembly, ACS Appl. Mater. Interfaces 10 (2026) 6895–6903, https://doi.org/10.1021/acsami.7b17327.

[47] J. Doyle, S. Uthicke, Sensitive environmental DNA detection via lateral flow assay (dipstick)—A case study on corallivorous crown-of-thorns sea star (*Acanthast er cf. solaris*) detection, Environ. DNA 3 (2026) 323–342, https://doi.org/10.1002/edn3.123.

[48] K. Fukaya, H. Murakami, S. Yoon, K. Minami, Y. Osada, S. Yamamoto, R. Masuda, A. Kasai, K. Miyashita, T. Minamoto, M. Kondoh, Estimating fish population abundance by integrating quantitative data on environmental DNA and hydrodynamic modelling, Mol. Ecol. 30 (2026) 3057–3067, https://doi.org/10.1111/mec.15530.